

Vibrational and crystalline properties of polymorphic CuInC_2 ($C=\text{Se,S}$) chalcogenides

J. Álvarez-García

Centre de Recerca i Investigació de Catalunya (CRIC), Margallo 12 (Les Planes), 08017 Barcelona, Spain

B. Barcones, A. Pérez-Rodríguez, A. Romano-Rodríguez, and J. R. Morante
*EME/CEMIC/CERMAE, Departament d'Electrònica, Universitat de Barcelona, Martí i Franquès 1,
 08028 Barcelona, Spain*

A. Janotti and Su-Huai Wei

National Renewable Energy Laboratory, Golden, Colorado 80401, USA

R. Scheer

Hahn-Meitner Institute, Glienicke Strasse 100, D-14109 Berlin, Germany

(Received 10 August 2004; published 15 February 2005)

This paper deals with the analysis of the vibrational and crystallographic properties of CuInC_2 ($C=\text{S,Se}$) chalcogenides. Experimentally, evidence on the coexistence in epitaxial layers of domains with different crystalline order—corresponding to the equilibrium chalcopyrite (CH) and to CuAu (CA)—has been obtained by cross section transmission electron microscopy (TEM) and high resolution TEM (HREM). Electron diffraction and HREM images give the crystalline relationship $[\bar{1}10]_{\text{CH}}\parallel[100]_{\text{CA}}$ and $(112)_{\text{CH}}\parallel(011)_{\text{CA}}$, observing the existence of a $(112)_{\text{CH}}\parallel(001)_{\text{CA}}$ interphase between different ordered domains. The vibrational properties of these polytypes have been investigated by Raman scattering. Raman scattering, in conjunction with XRD, has allowed identifying the presence of additional bands in the Raman spectra with vibrational modes of the CA ordered phase. In order to interpret these spectra, a valence field force model has been developed to calculate the zone-center vibrational modes of the CA structure for both CuInS_2 and CuInSe_2 compounds. The results of this calculation have led to the identification, in both cases, of the main additional band in the spectra with the total symmetric mode from the CuAu lattice. This identification is also supported by first-principles frozen-phonon calculations. Finally, the defect structure at the interphase boundaries between different polymorphic domains has also been investigated.

DOI: 10.1103/PhysRevB.71.054303

PACS number(s): 78.30.Fs, 81.05.Dz, 68.55.Nq, 61.66.Fn

I. INTRODUCTION

The $\text{Cu-B}^{\text{III}}\text{-C}_2^{\text{VI}}$ family of compounds, and in particular CuInC_2 with $C=\text{Se,S}$, are currently under development for optoelectronic applications such as solar cells.¹⁻⁵ These ternary compounds are derived from the $\text{II}_2\text{-VI}_2$ sphalerites and belong to the group of nonisovalent ionic semiconductors⁶ where two group II atoms are replaced by one Cu and one group III atom. The nonisovalent cations form an ordered sublattice at room temperature. Locally, the crystal structures of $\text{Cu-B}^{\text{III}}\text{-C}_2^{\text{VI}}$ contain tetrahedra of the $\text{Cu}_n\text{B}^{\text{III}}_{(4-n)}$ ($n=1,2,3,4$) type which are formed around a common C atom. Wei *et al.* have shown that energy minimization can be realized if $n=2$. In that case the octet rule is fulfilled.⁷ The ordering of highest thermodynamical stability at low temperature gives rise to the chalcopyrite structure (CH) with space group ($I42d$) and $n=2$.⁷ The CuAu (CA) ordering ($P4m2$) is most closely related to the CH ordering as it also exhibits $n=2$. The formation energies of CH and CA differ only by 2 meV/atom.⁸ Other structures exhibiting $n=1$ and $n=3$ tetrahedra [CuPt ordering ($R3m$) or Y2-like ordering] are thermodynamically less stable. Early reports on their existence in CuInSe_2 thin films have not yet been confirmed.⁹ It shall be emphasized that all polytypes are only different with respect to their cation sublattice but have an identical fcc chalcogen sublattice.

Recently, experimental evidence was provided that two different orderings with $n=2$ can be differentiated by studying their vibrational properties using Raman scattering.¹⁰⁻¹² This is related to the presence of additional modes in the Raman spectra, which have been attributed to the presence of CuAu ordered domains in both epitaxial and polycrystalline films. Despite the fact that the Raman spectra of the CH ordered phases of CuInC_2 compounds are well-known,^{10,13,14} very few works have been reported on the analysis of the dynamical properties of the CA ordered phase.^{10,15} In these works, even if there is consensus in attributing the additional peaks in the Raman spectra to the vibrational modes from the CA ordered phase, the identification of the main CA mode is still not clear: although the experimental results in both CuInSe_2 and CuInS_2 have led to the identification of this peak with an A_1 vibrational mode,^{12,16} and in the case of CuInS_2 previous theoretical considerations have confirmed this assignment,¹⁰ more recently the theoretical calculation performed by Lazewski *et al.* on the lattice dynamics of CA ordered CuInSe_2 have led them to identify this peak with an E_2 mode.¹⁵ To clarify this, it appears worthwhile to calculate and compare the zone-center phonon spectra of the CA structure for both CuInC_2 ($C=\text{S,Se}$) compounds.

Phenomenological studies have shown that the formation of CA metastable domains in mostly CH ordered thin films is related to a deterioration of their optoelectronic

properties.^{11,17} Therefore, the elucidation of polytypic structures in Cu- B^{III} - C_2^{VI} materials is important from a fundamental as well as an applicational point of view. Also of physical interest is the defect structure at interphase boundaries between two polytypes, i.e., between the $n=2$ polytypes CA and CH. At these boundaries, which we refer to as interphase boundaries (IPB), tetrahedra with $n \neq 2$ may be forming. Tetrahedra with $n > 2$ ($n < 2$) exhibit a deficiency (an excess) of valence electrons. Thus they can be considered as defect tetrahedra of acceptor (donor) character. Wei *et al.* have stated that donor and acceptor type tetrahedra can couple⁷ leading to donor-acceptor complexes. It has been pointed out that tetrahedra with $n \neq 2$ may be compensating each other in the disordered high-temperature zinc blende-type modification of the Cu chalcopyrites.⁷

This paper presents a comprehensive study on the subject of ordering in Cu- B^{III} - C_2^{VI} materials and the implications on the vibrational and crystalline properties. It is organized as follows: In the next section, the experimental evidence for polytypes in CuInC₂ with $C=\text{Se,S}$ obtained from crystallographic and vibrational studies is presented. In the third section, it shall be asked if the experimentally revealed vibrational properties of CuInC₂ solids can be interpreted in terms of their polymorphic structure. A valence force field model will be employed for the comparison of CA and CH lattice dynamics. The results from this model will be also compared with those from first-principles frozen-phonon calculations. The last section focuses on the coexistence of CA and CH domains in solid specimens and the defect structure within interphase boundaries, investigating the nature that can be predicted for these defects and the possible charging states of low indexed IPBs.

II. EXPERIMENTS

A. Experimental details

The experimental data have been obtained from epitaxial CuInS₂ and CuInSe₂ samples prepared by molecular beam epitaxy.^{18,19} The substrates were [111] and [001] oriented Si for the [221]-CuInS₂ and [001]-CuInS₂ specimens, and [100] oriented GaAs for the [001]-CuInSe₂ epilayers. By means of a variation of the substrate temperature it was possible to grow epitaxial films of different crystallographic properties. The thickness of these epilayers was typically around 200–500 nm.

Cross-section transmission electron microscopy (TEM) and transmission electron diffraction (TED) experiments were performed in a Philips CM30ST microscope, operating at 300 kV. Micro-Raman measurements were carried out in a T64000 Jobin Yvon equipment, using different excitation lines of an Ar⁺ laser (514.5, 488, and 457.9 nm) as light excitation source. Finally, x-ray diffraction (XRD) measurements were performed in a Philips MRD diffractometer, using its parallel beam optics.

B. Crystalline structure of polytypic CuInC₂

[221]-CuInS₂ epitaxial layers grown on Si [111] substrates were studied by cross-section TEM in the perpendicular

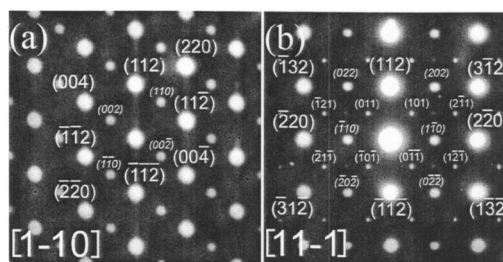


FIG. 1. Electron diffraction patterns obtained from a CuInS₂ epilayer in the $[1\bar{1}0]_{\text{CH}}$ and $[1\bar{1}1]_{\text{CH}}$ directions. The plane indexes are related to the CH structure, and those indicated in italics are forbidden for the CH structure but allowed for the CA one.

directions $[1\bar{1}0]$ and $[1\bar{1}1]$. The diffraction patterns shown in Fig. 1 are taken in these directions and confirm that in this case the CuInS₂ layers are grown in the $[221]_{\text{CH}}$ direction. These patterns show, in addition to the spots allowed for the chalcopyrite structure in these directions, additional spots that correspond to $(002)_{\text{CH}}$ and $(110)_{\text{CH}}$ planes in the $[1\bar{1}0]_{\text{CH}}$ direction [Fig. 1(a)] and to $(110)_{\text{CH}}$, $(202)_{\text{CH}}$, and $(022)_{\text{CH}}$ planes in the $[1\bar{1}1]_{\text{CH}}$ direction [Fig. 1(b)]. These diffraction spots are forbidden in the chalcopyrite structure, due to its systematic extinctions. On the other hand, they are compatible with ordering of the cations into planes following the $[001]_{\text{CH}}$ direction, and filling the $(002)_{\text{CH}}$ planes alternately with only one type of cations Cu or In. This structure corresponds to the so-called CuAu-ordering. Other authors have described the CuAu-ordering with Cu and In planes in the $[010]_{\text{CH}}$ direction, assuming the IPB contains only $n=2$ tetrahedra.^{7,20} However, in such a case the additional spots in Fig. 1 would correspond to planes $(020)_{\text{CH}}$, $(102)_{\text{CH}}$, $(210)_{\text{CH}}$, and $(014)_{\text{CH}}$, respectively, and these planes cannot be observed in the $[1\bar{1}0]_{\text{CH}}$ and $[1\bar{1}1]_{\text{CH}}$ directions. Therefore, the presence of these spots in the diffraction patterns obtained within these directions can only be interpreted in terms of coexistence of CuAu and CH ordering assuming that the C axes of both unit cells are parallel. This is also consistent with the XRD experimental spectra reported by Stanbery *et al.*¹² on CuInSe₂ epilayers, that are interpreted assuming that the alternating Cu and In cation planes are oriented parallel to the (001) plane of the epitaxial chalcopyrite structure. Figure 2 shows the corresponding CH and CA primitive unit cells. For these unit cells the diffraction patterns in Fig. 1 lead to the crystalline relationship $[1\bar{1}0]_{\text{CH}} \parallel [100]_{\text{CA}}$ and $(112)_{\text{CH}} \parallel (011)_{\text{CA}}$.

Figure 3 shows a dark field transmission electron image and its diffraction pattern recorded along the $[1\bar{1}0]$ zone axis of the chalcopyrite lattice. Figure 3(a) shows the electron diffraction pattern from the area in Fig. 3(b). This pattern exhibits the spots already described in Fig. 1(a) together with doubled spots which are due to twins in the direction $[22\bar{1}]_{\text{CH}}$. In addition, the main CH reflections from Figs. 1 and 3 show streaking along $[221]_{\text{CH}}$ and $[22\bar{1}]_{\text{CH}}$ directions, which are due to stacking faults formed in the (112) and $(1\bar{1}2)$ planes of the CH structure.²⁰ In Fig. 3, the spots are labeled according to their corresponding structure (CH or CA), in contrast to Fig. 1 where all the spots were labeled according to the CH structure. In this figure, the twinned

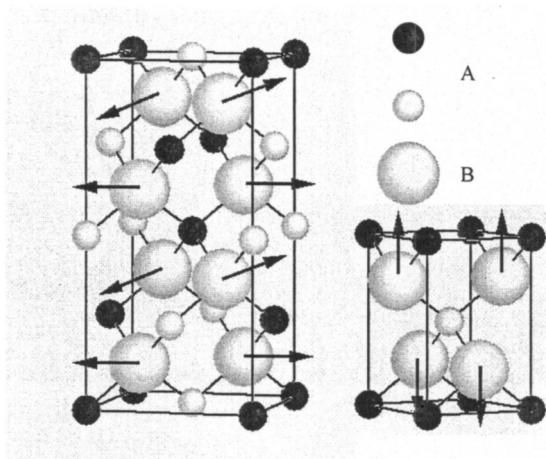


FIG. 2. Chalcopyrite (left) and CuAu ordering (right) primitive cells. The arrows indicate the atomic displacements of the anions corresponding to the A_1 vibration in both structures, as described in Sec. II C.

spots are marked by crosses. Apart of these defects, which are very common in chalcopyrite structure materials, all the spots in this figure can be ascribed to the crystalline relationship already mentioned between the CH and CA lattices. Only some weak spots in Fig. 1(b) have not been indexed. The origin of these spots is still not clear, and could indicate the existence of domains with different crystalline orientation or secondary phases, or other polytypes of CuInC_2 such as primitive chalcopyrites.⁸ Nevertheless, these spots have a much lower intensity than those related to both CA and CH structures. The dark field image in Fig. 3(b) was obtained by selecting the $(001)_{\text{CA}}$ beam, which is forbidden for the CH structure but is allowed for the CA structure. This image shows the spatial distribution of CH and CA ordered domains. So, the upper grain in the image corresponds only to CA ordered CuInS_2 , and it shows an interphase boundary with the underlying CH domain formed by $(112)_{\text{CH}}$ and $(011)_{\text{CA}}$ planes (indicated with an arrow). Figure 4 shows a filtered high-resolution TEM (HREM) image taken along the $[1\bar{1}0]_{\text{CH}}$ zone axis from a $(112)_{\text{CH}} \parallel (011)_{\text{CA}}$ interphase region. The corresponding Fourier transform (down left inset)

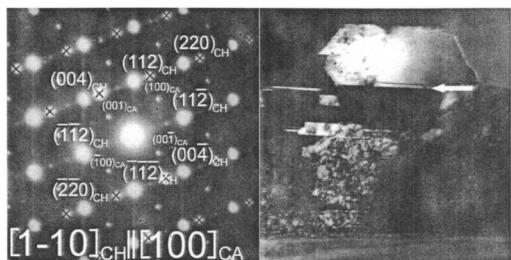


FIG. 3. TEM images obtained from a CuInS_2 epilayer containing CA-ordered domains. (a) Electron diffraction pattern. This pattern exhibits the spots already described in Fig. 1(a) together with doubled spots (marked with crosses) which are due to twins in the direction $[1\bar{1}1]_{\text{CH}}$. (b) Dark field image formed using the characteristic CA diffraction spot $(001)_{\text{CA}}$. The arrow in this image shows an interphase boundary defined by the planes $(112)_{\text{CH}} \parallel (011)_{\text{CA}}$.

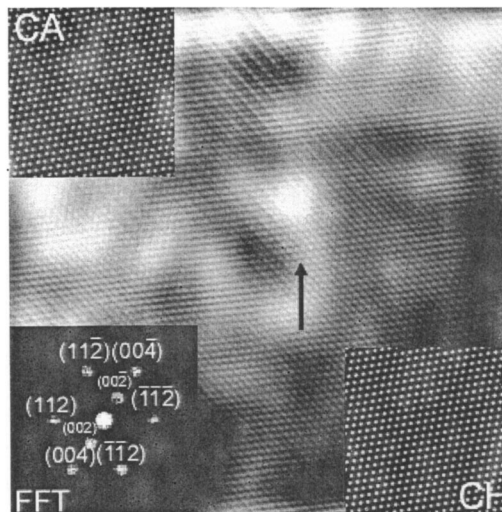


FIG. 4. Filtered HREM image taken along the $[1\bar{1}0]_{\text{CH}}$ zone axis corresponding to the crystallographic interface defined by the planes $(112)_{\text{CH}} \parallel (011)_{\text{CA}}$. For more clarity, an arrow is included in the plane of the interphase. The corresponding fast Fourier transform (FFT) and the HREM simulation are given in the insets of the image.

agrees with the electron diffraction pattern previously shown in Fig. 1(a). The other insets in this figure show the respective HREM simulations for both structures. Although the interphase is difficult to see visually in the image, the agreement between these simulations and the respective regions in the image corroborates the coexistence of both orderings within the characteristic interphase boundary.

C. Raman active modes of polytypic CuInC_2

It has been reported earlier that Raman spectra of the A_1 mode of CuInC_2 samples often show an additional band slightly higher in wave number as compared to the A_1 mode of CH.¹⁰⁻¹² Figure 5 gives examples of the respective spectral region of the A_1 mode for different samples of CuInS_2 and CuInSe_2 . Notice that other modes are difficult to resolve due to their low Raman scattering efficiency. The dominant bands at about 300 and 175 cm^{-1} for CuInS_2 and CuInSe_2 , respectively, are composed out of two modes. Curve fitting was used to derive the different wavenumber contributions to be 290 and 305 cm^{-1} for CuInS_2 and 173 and 183 cm^{-1} for CuInSe_2 . It can be clearly seen that the spectra differ with respect to the ratio of their two components. From the fit results this ratio has been quantified.

Raman spectroscopy in conjunction with XRD analysis has been used for the qualification of CA ordered domains in CuInS_2 .¹⁰ This analysis has allowed observing a direct correlation between the relative intensity of the 305 cm^{-1} vibrational mode and the amount of CA ordered phase in the samples, as determined by XRD. In the following, similar experimental evidence is provided that the 183 cm^{-1} component in the spectra measured in the CuInSe_2 specimens originates from a volume share of CA ordered domains in the films. The procedure is based on combined XRD/Raman measurements as the CH and CA tetragonal structures can be

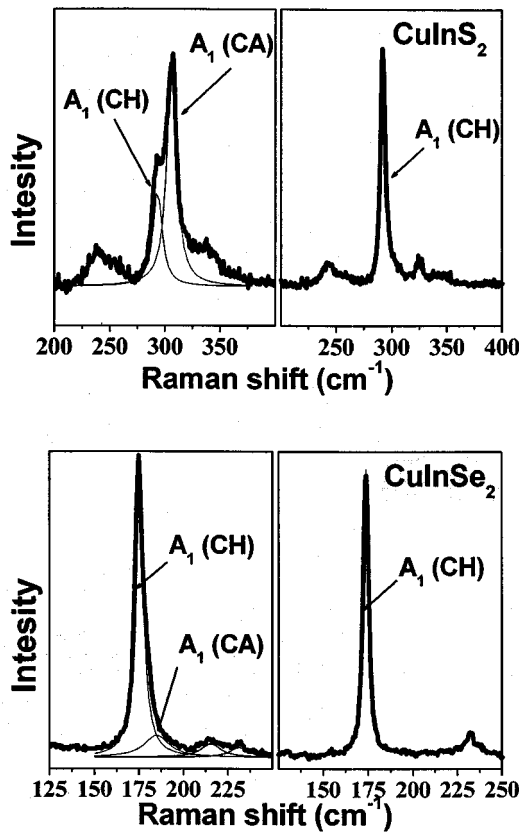


FIG. 5. Raman spectra of CuInS₂ (a) and CuInSe₂ (b) films presenting only chalcopyrite ordering (right) and a mixture of CH and CA polytypes (left), together with the respective fitting with modes attributed to CA and CH ordered phases.

distinguished by their characteristic x-ray diffractograms. Since the CA unit cell is primitive and its crystal space group contains no glide planes or screw axis, there are no systematic extinctions in the CA diffractogram. Therefore the (001) and (003) reflections, which are forbidden for the CH structure, are characteristic reflections of the CA structure (in this section cubic notation for the Miller indexes are used throughout). In the case of epitaxial layers containing CA domains (as confirmed by their TEM analysis), we have been able to accurately measure these reflections by tilting the samples. The intensity of each XRD band was evaluated from the integral area of the band after fitting the peak with a Voigt function.

Figure 6 shows the Raman peak ratio from the spectra measured in the CuInSe₂ films as a function of the relative XRD intensity between the (003) reflection, characteristic of the CA structure, and the (004) reflection arising from both CA and CH structures. The intensity ratio $I(003)/I(004)$ is therefore a direct measurement of the relative amount of CA phase within the samples (see Ref. 10 for further details). A linear correlation between both quantities is revealed which proves that the intensity of the additional band is directly related to the fraction of CA within the films. This agrees with the behavior observed for CuInS₂.

Stanbery¹² and Lazewsky¹⁵ have reported the possible existence of resonant or preresonant effects in the Raman spec-

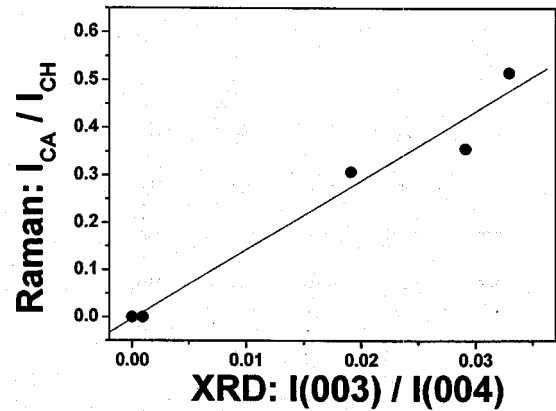


FIG. 6. Relative intensity of the CA CuInSe₂ Raman band versus XRD intensity ratio between (003) and (004) reflections.

tra from CuInSe₂ measured with excitation wavelength of 514 nm. These authors argued that these resonant conditions were responsible for the breakdown of the selection rules, and the observation of some modes which are expected to be forbidden in some experimental polarization configurations. In order to confirm the symmetry characteristics of the modes, we have performed polarization-dependent measurements using different excitation lines: 514.5, 488, and 457.9 nm. Figure 7 shows the spectra measured on a CuInSe₂ sample under parallel (A_1 allowed) and perpendicular (A_1 forbidden) configurations with 457.9 nm excitation wavelength. For these configurations, E modes would be forbidden in both cases. Although for the samples analyzed in this work the intensity of the additional mode in the Raman spectra is not high enough to obtain spectral resolution of the peaks, the spectra in Fig. 7 clearly demonstrate the existence of a similar behavior to that of the well-known CH A_1 mode. The spectrum measured using $\langle z|xx|\bar{z} \rangle$ configuration is very similar to those measured focusing the laser spot on the cross section surface of the layers (where, in principle, E modes would not be forbidden). On the other hand, the spectra measured with different excitation wavelengths indicate the absence in these measurements of resonant effects. In spite of

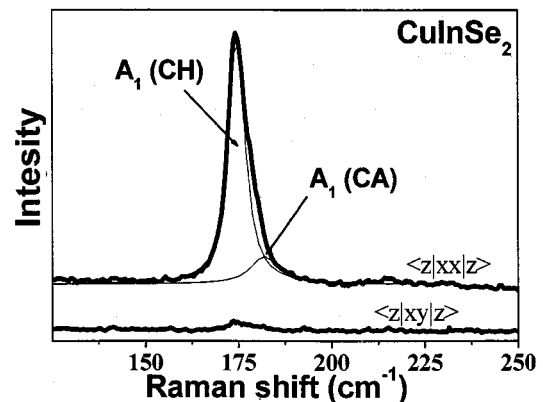


FIG. 7. Polarized Raman spectra of a CuInSe₂ layer exhibiting both CH and CA contributions measured with 457.9 nm excitation wavelength using $\langle z|xx|\bar{z} \rangle$ and $\langle z|xy|\bar{z} \rangle$ configurations ($x=[110]$, $y=[\bar{1}\bar{1}0]$ and $z=[001]$ using cubic notation of Miller indexes).

the low intensity of the mode in the spectra, its spectral position agrees with that previously reported for the additional CA related band. These data, and the clear correlation between the relative intensity of this contribution and that of the CA content in the samples—as described in the previous paragraph—lead to the identification of this contribution in the spectra with the A_1 mode from CA ordered CuInSe_2 .

III. LATTICE DYNAMICS: CALCULATION OF ZONE CENTER VIBRATIONAL MODES

In order to understand the Raman spectra of CuInS_2 and CuInSe_2 films, it is necessary to first consider the dynamical properties of the CH and the CA crystallographic structures. The eight atoms per unit cell in the chalcopyrite lattice lead to the existence of 24 normal modes at the zone-center (point Γ) of the Brillouin zone, and thus 21 optical phonons. The character table of the chalcopyrite point group D_{2d} includes five different types of irreducible representations A_1 , A_2 , B_1 , B_2 , and E . Each representation is defined by their characters for each operation. All the representations in the group D_{2d} are single-degenerated, except the representation E which is doubly degenerated. Triple-degenerated representations do not exist in the point symmetry group of the crystal, due to the inequivalence of the X - Y and Z directions. In the case of the chalcopyrite structure, the Cu and In atoms occupy a type Wyckoff sites (site symmetry S_4) and the anions occupy d type sites (site symmetry C_2). With the previous information, the correlation method²¹ gives the following irreducible representations of the zone-center phonons in the chalcopyrite structure

$$\Gamma_{\text{opt}} = A_1 \oplus 2A_2 \oplus 3B_1 \oplus 3B_2 \oplus 6E, \quad (1)$$

$$\Gamma_{ac} = B_2 \oplus E.$$

All the chalcopyrite optical modes are Raman active, except the A_2 modes that are “silent.” B_2 and E modes exhibit LO-TO splitting, due to their polar character. On the other hand, the decomposition of the zone-center phonons for the CA structure into irreducible representations is different from the CH case. Although the crystal point group is also D_{2d} , the CA structure contains a single molecule per unit cell. Therefore, there exist only nine optical modes that can be arranged according to group theory in the following way:

$$\Gamma_{\text{opt}} = A_1 \oplus 2B_2 \oplus 3E, \quad (2)$$

$$\Gamma_{ac} = B_2 \oplus E.$$

Since the crystallographic group of the CA is not a supergroup of the CH structure, a simple branch folding scheme is not appropriate to predict the phonon spectra of the CA structure. Instead, we use the Keating model^{22,23} to calculate the zone-center vibrations in the CuInC_2 crystal. This is a particular case of the “valence force field” (VFF) models, and was first developed by Keating, who applied invariance requirements to the strain energy of the diamond crystal to derive a mathematical form for the elastic potential, which is given by the expression

$$U = \frac{1}{2} \alpha \left(\frac{3}{4r^2} \right) \sum_{i=1}^4 [\Delta(r_i^l r_i^l)]^2 + \frac{1}{2} \sum_{s=1}^{s=2} \beta^s \left(\frac{3}{4r^2} \right) \sum_{i=1}^4 [\Delta(r_i^s r_i^s)]^2. \quad (3)$$

Here, the vectors \vec{r}_i^s correspond to the vectors joining the atoms s and its first neighbor i , and the elastic potential between atoms is described by the squares of the variation of the dot products $\Delta(\vec{r}_i^s \cdot \vec{r}_j^s)$. α and β constants correspond to the stretching and bending force constants, respectively.

Within this approximation, five bond-bending constants are needed in order to describe the interactions [Cu-C-Cu, In-C-In, In-C-Cu, C-Cu-C, C-In-C], while the other two stretching constants are required for the stretching interactions between Cu-C and In-C. Therefore, it is important to be able to find physical arguments to achieve a further reduction in the number of constants of our model. This can be done by assuming the following hypothesis. (1) The bond-bending force constants for a given set of atoms including only two types of atoms will be the same, independently of which atom is in the center and which atoms are in the edges (in this way, the interactions Cu-C-Cu and C-Cu-C are described by a single constant β_1 , and the interactions In-C-In and C-In-C by a constant β_2). (2) For the sets of atoms of the type Cu-C-In the bond-bending interaction is assumed to correspond to the arithmetic average of the bond-bending constants describing the sets Cu-C-Cu and In-C-In. Therefore, $\beta_{12} \approx 1/2(\beta_1 + \beta_2)$. This reduces the number of constants needed to describe the elastic interactions in the chalcopyrite lattice to two stretching constants for the Cu-S(Se) and In-S(Se) interactions (α_1 and α_2 , respectively) and two bond-bending constants (β_1 and β_2). Within this approach, the phonon spectra can be calculated by solving the 24×24 dynamical matrix.

In order to calculate the phonon spectra of the CA structure, we will apply the Keating model first to the chalcopyrite crystal, whose experimental frequencies are already well-known.^{10,13,14} From the experimental data, the force constants involved in the model can be extracted. Once the values of the force constants are known, they will be used to calculate the expected frequencies for the CA-ordered crystal. We will assume that the bond distances and bond angles of both crystal orders are similar, and therefore that it is not necessary to rescale the force constants. Actually, no important differences are expected due to the strong relationship between both structures, and because the atoms constituting the crystal are the same and they are tetrahedrally coordinated in both cases. Unfortunately, experimental results are not available to confirm this assumption. However, it has been shown that the introduction of vacancies in the chalcopyrite structure leads to the formation of ordered vacancy compounds (OVC) which keep the same interatomic chalcopyrite distances within an error of 0.01 Å, as determined by EXAFS.²⁴ It is unlikely that the rearrangement of the cations in the cation sublattice could modify the bond parameters in a more important way than the introduction of vacancies.

The determination of the force constants has been accomplished by optimizing their values in order to reproduce the

TABLE I. Experimental (Refs. 10, 13, and 14) and calculated modes within the VFF model for the chalcopyrite CuInS₂ and CuInSe₂.

Mode	Transversal optical modes			
	CuInS ₂ ω_{exp} (cm ⁻¹)	ω_{Keating} (cm ⁻¹)	CuInSe ₂ ω_{exp} (cm ⁻¹)	ω_{Keating} (cm ⁻¹)
$B_2^1 [\Gamma_{15}]$	321	328	215	231
$E^1 [\Gamma_{15}]$	323	324	217	230
$A_2^1 [X_1]$	(silent) ^a	294	(silent) ^a	182
$B_1^1 [W_2]$	(very weak) ^a	293	229	220
$E^2 [W_4]$	295	290	227	221
$B_2^2 [W_2]$	234	253	177 (100 K) ^a	215
$A_1 [W_1]$	290	253	173	163
$E^3 [X_5]$	244	246	211	212
$A_2^2 [W_1]$	(silent) ^a	214	(silent) ^a	150
$B_1^2 [X_3]$	157	156	179	163
$E^4 [W_3]$	140	149	188 (100 K) ^a	157
$E^5 [W_4]$	88	84	77	70
$B_1^3 [W_1]$	(very weak) ^a	81	67	68
$B_2^3 [W_2]$	79	79	70	69
$E^6 [X_5]$	67	70	58	61

Force constants (dyn/cm)

$\alpha_1 = 18.16 \times 10^3$ $\beta_1 = 1.09 \times 10^3$ $\alpha_1 = 22.72 \times 10^3$ $\beta_1 = 1.08 \times 10^3$
 $\alpha_2 = 37.51 \times 10^3$ $\beta_2 = 1.26 \times 10^3$ $\alpha_2 = 35.14 \times 10^3$ $\beta_2 = 1.25 \times 10^3$

^aThese modes were not used in the fitting.

experimental phonon spectra. Therefore, by using the experimental values of the different CuInS₂ and CuInSe₂ modes reported in the literature, the problem restricts to the minimization of the function χ^2 , defined as the quadratic deviation of all the experimental values with respect to the values predicted by the Keating model

$$\chi^2(\alpha_1, \alpha_2, \beta_1, \beta_2) = \sum (\omega_j^{\text{Experimental}} - \omega_j^{\text{Keating}})^2. \quad (4)$$

The optimization of the values of the phenomenological force constants has been carried out using the SIMPLEX algorithm, which proved good convergence towards a unique, real, and stable solution, independently of the initial conditions. The experimental transversal optical frequencies used in the fitting are compared with the results obtained from the four parameters Keating model in Table I. The modes have been classified according to their symmetry, and the point in the Brillouin zone of the zinc blende where they come from after folding it back is indicated in square brackets. The table also includes the optimum values of the force constants.

The values for the force constants obtained by this method are reasonable in terms of their physical meaning. They are all positive, which is expectable from their definition. Notice also that the values for the stretching force constants are one order of magnitude greater than the values for the bond-bending constants, and that the corresponding constants involving In-C interactions are greater than those involving Cu-C interactions, i.e., $\alpha_2 > \alpha_1$ and $\beta_2 > \beta_1$, as one

may expect due to the higher strength of the In-C bond. On the other hand, Table I also shows that the Keating model is able to reproduce with good accuracy the experimental results, despite the low number of parameters used for the description of the interactions. Most of the predicted frequencies agree with the experimental ones within an error of about 5%. It is worth noting that the predicted position for the A_1 mode of CuInS₂ has a higher relative deviation from the experimental position of the mode, of almost 13%. This is a common limitation of this model, and has been already reported in the literature for other compounds.²⁵ It is clear that second neighbor interactions should be taken into account if one wishes to find with more accuracy the frequency of the A_1 mode.

Once we determined the optimum values of the force constants used in the VFF model, we used these values for calculating the phonon spectra of the CA structure for these compounds. The results of these calculations are given in Table II. Before attempting to compare the experimental frequencies of the modes with the results obtained using the VFF model, we should take into account the absolute uncertainty in the position of the A_1 modes. For instance, for CuInS₂ the Keating model predicts the position of this band to be 253 cm⁻¹ for the CH structure, and 266 cm⁻¹ for the CA crystal. Thus, if we consider that the experimental frequency of the CH mode is 290 cm⁻¹, we would expect the frequency of the CA A_1 mode to be $\omega[A_1^{CA}] \approx \omega_{\text{Keating}}^{CA} / \omega_{\text{Keating}}^{\text{CH}} \times 290 \text{ cm}^{-1} = 305 \text{ cm}^{-1}$, which is in excellent agreement with the experimental

TABLE II. Calculated zone-center phonons for the CA structures of CuInS₂ and CuInSe₂.

Mode	Transverse optical phonons in CA order structures	
	CuInS ₂	CuInSe ₂
	$\omega_{\text{Keating}}^{\text{CA}}$ (cm ⁻¹)	$\omega_{\text{Keating}}^{\text{CH}}$ (cm ⁻¹)
E^1	325	231
B_1^1	295	226
A_1	266	171
E^2	246	213
B_2^2	157	163
E^3	82	62

findings. Likewise, for CuInSe₂ we obtain good results after correcting the absolute value of the frequency of the mode: $\omega[A_1^{\text{CA}}] \approx \omega_{\text{Keating}}^{\text{CA}} / \omega_{\text{Keating}}^{\text{CH}} \times 173 \text{ cm}^{-1} = 182 \text{ cm}^{-1}$. Because these compounds have very low Raman scattering efficiency, it is difficult to identify other CA bands in the spectra of these films. Only the A_1 band appears to be intense enough for being clearly resolved from the CH bands under standard measurement conditions.

It is worth noting that the frequency of the totally symmetric mode in both crystalline structures (CH and CA) is very similar, since in both cases it arises from the movement of the anions, with all the cations remaining at rest. Nevertheless, the vibrational frequency of the A_1 mode in each structure is still different, since the vibrational energy associated with the respective atomic displacement is not the same. Atomic displacement eigenvectors can be readily obtained by using the corresponding projector operators. In the CH structure, two of the four anions in the atomic base move along the X crystallographic direction antiparallel to each other, while the other two anions move in the same way following the Y crystallographic direction (Fig. 2). However, in the case of the CA structure, all the anion displacements occur along the Z crystallographic direction, with alternate atomic planes moving also antiparallel to each other. Therefore, the A_1 vibration in the case of the CA structure is associated with a larger bond bending distortion on the bonds with a vertex at the cation site, since the antiparallel displacement of the four anions in the tetrahedra occurs along the same direction. This argument, based on crystallographic symmetry, explains why the A_1 frequency in the CA structure is higher than that in the CH structure. Furthermore, because the elastic constants of CuInSe₂ are smaller than CuInS₂ due to the larger volume of CuInSe₂, the A_1 frequency difference between the CA and CH modes in CuInSe₂ is also smaller than that in CuInS₂.

The assignment of the main vibrational mode from CA ordered CuInSe₂ with the A_1 mode does not agree with Lazewski *et al.*,¹⁵ who have identified the peak at 183 cm⁻¹ in the spectra with the E^2 (LO) mode from CA structure that, according to their calculation, appears at 177 cm⁻¹. They assigned the CA A_1 mode with a much weaker peak in the spectra, experimentally observed at 195 cm⁻¹. These authors

have claimed the existence of resonance effects to justify the disagreement with the spectra measured under different polarization conditions, which show a totally symmetric behavior for the 183 cm⁻¹ peak.¹² However, we have observed that even when the measurements are performed at excitation conditions away from resonance ($\lambda_{\text{exc}} = 457.9 \text{ nm}$) polarization measurements still show a totally symmetric behavior for this mode. On the other hand, some of the calculated frequencies in the CA structure have a clear equivalence in the CH lattice. Specifically, all the E -symmetry modes in the CA: E^1 , E^2 , and E^3 lie at spectral positions very close to E^1 , E^3 , and E^6 modes of the CH, respectively, thus indicating the strong equivalence of these vibrations in terms of vector displacements. However, the spectral positions of B_2 modes in the CA lattice do not have a clear equivalence in the CH structure, thus revealing the difference in both crystallographic structures and the fact that it is not possible to establish a direct group/subgroup relation between them. Such relations between the CH and CA modes can be found also in the results provided by Lazewski *et al.*,¹⁵ although these authors reported different values for the calculated frequencies in the CA structure of CuInSe₂. Direct comparison of the numerical results provided by both models with the experimental values reported in the literature show that the average relative error in the determination of the frequency of the modes in the chalcopyrite structure is 6.9 and 11.6 % for the Keating model used in this work and the *ab initio* calculations performed by Lazewski, respectively. In the case of the calculations for the CA structure, the lack of experimental data on pure CA-ordered crystals does not allow for such a comparison. Moreover, taking into account the physicochemical complexity of CuIn_xSe_y compounds, assignment of weak modes based on nonpolarized Raman experiments on multiphase samples, as proposed by Lazewski, appears doubtful.

In the case of CuInS₂, the symmetry assignment of the main vibrational mode from the CA ordered phase deduced from the VFF model was supported by first-principles phonon calculations performed using the frozen phonon approach.¹⁰ These calculations were made assuming a totally symmetric A_1 mode related to the vibration of the chalcogen atoms. We have performed this calculation under the same conditions as those reported in Ref. 10 for CuInSe₂ in both CH and CA structures. In this case, the calculated frequencies are 179 and 189 cm⁻¹ for the CH and CA structures, respectively. These values are slightly higher than the experimental ones, because the local density approximation used in the calculation underestimates the lattice constants by ~1% and slightly overestimates the force constants. In spite of this, we have to remark the agreement of the difference predicted by the calculation in the modes from both CA and CH structures with the experimental data, which gives support to the symmetry assignment deduced from our VFF calculation.

IV. INTERPHASE BOUNDARIES

The experimental evidence obtained on the coexistence of CH and CA ordered domains with a specific interphase raises the question on the nature of the domain boundaries which

TABLE III. Interphase boundaries (IPB's) between different CH and CA ordered planes and the tetrahedra occurring at these boundaries. The quantity $[A]-[B]$ gives the difference between the number of atoms A and atoms B in the tetrahedra of one interface unit cell. The IPB can contain compensated defects (C) or uncompensated defects (U).

APB	Tetrahedra	$[A]-[B]$	Type
$(112)_{\text{CH}}/(011)_{\text{CA}}$	$A_3B+2A_2B_2$ $+AB_3$	0	C
$(100)_{\text{CH}}/(110)_{\text{CA}}$	$A_3B+2A_2B_2$ $+AB_3$	0	C
$(001)_{\text{CH}}/(001)_{\text{CA}}$	$2A_3B(2AB_3)$	$4(-4)$	U
$(010)_{\text{CH}}/(\bar{1}10)_{\text{CA}}$	$A_3B+2A_2B_2$ $+AB_3$	0	C
$(110)_{\text{CH}}/(010)_{\text{CA}}$	$2A_3B$ $+2A_2B_2(2AB_3$ $+2A_2B_2)$	$2(-2)$	U

may be considered as interphase boundaries (IPB's). Both the CH and the CA structure comply with the octet rule: they only contain tetrahedra of the A_2B_2 type. We constructed the following IPB's between a CA substrate and a CH overlayer where we assumed that the octet rule is being regarded within each of the two domains. Thus, our considerations make use of a rigid domain model. Furthermore, we assumed the coherence of the anion fcc sublattice across any domain boundary. We have restricted this study to IPBs formed by the planes of low index that are consistent with the crystalline relationship $[1\bar{1}0]_{\text{CH}}\parallel[100]_{\text{CA}}$ and $(112)_{\text{CH}}\parallel(011)_{\text{CA}}$ deduced from the electron diffraction patterns. These correspond to the interphase boundaries formed by the planes $(112)_{\text{CH}}$ and $(011)_{\text{CA}}$, $(100)_{\text{CH}}$ and $(110)_{\text{CA}}$, $(001)_{\text{CH}}$ and $(001)_{\text{CA}}$, $(010)_{\text{CH}}$ and $(\bar{1}10)_{\text{CA}}$, and $(110)_{\text{CH}}$ and $(010)_{\text{CA}}$. For these boundaries, different types of tetrahedra can be deduced by means of geometric considerations. Their types are listed in Table III. Figure 8, in addition, depicts the tetrahedra found in the interface unit cell of a specific IPB.

As revealed in Table III, none of the investigated IPB's can be formed without breaking the octet rule. In all cases tetrahedra with $n \neq 2$ have to be formed. All but two IPB's in this table exhibit an equal number of A and B atoms. Thus, formation of these IPB's can lead to full compensation (denoted by C in the table) of donor and acceptor type of tetrahedra. Accordingly, the net charge of ionized donor type and acceptor type tetrahedra is zero. The defect tetrahedra in these interfaces may not contribute to a specific excess of charge carriers within this material. This is the case for the interface experimentally detected from the TEM analysis of the films, as discussed in the previous section. The $(001)_{\text{CH}}/(001)_{\text{CA}}$ and the $(110)_{\text{CH}}/(010)_{\text{CA}}$ IPB's, however, can be formed with an excess of A or B atoms. In the rigid domain model applied here, these interfaces cannot be compensated. Therefore, such an IPB may be charged leading to band bending and doping of the adjacent domains. However, several crystallographic mechanisms may compensate the electric charge associated to these IPB's. One possible compensation mechanism is the formation in the material of multiple

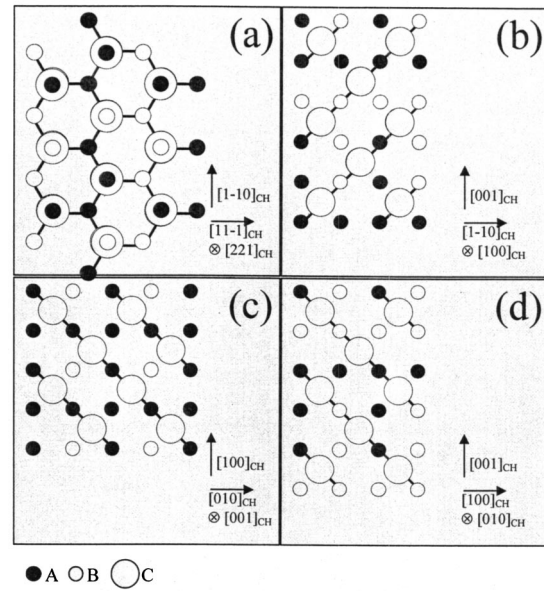


FIG. 8. Graphical representation of different IPB's between a CA ordered domain (bottom layer) and a CH ordered one (top layer). Only the bonds in the bottom layer are depicted. (a) $(112)_{\text{CH}}$ on $(011)_{\text{CA}}$, (b) $(100)_{\text{CH}}$ on $(110)_{\text{CA}}$, (c) $(001)_{\text{CH}}$ on $(001)_{\text{CA}}$, (d) $(010)_{\text{CH}}$ on $(110)_{\text{CA}}$.

IPB's of different excess type. Moreover, charge compensation may be accomplished also through the formation of complex point defects involving substitutional atoms and vacancies. A well-known example of such defect is the compensation of the local deficiency of the Cu atoms through the formation of In related complex defects with very low formation energies as $(\text{In}_{\text{Cu}}+2V_{\text{Cu}})$,²⁶ which allows preserving the stoichiometry of the crystal. Through the formation of these complex defects, the $\text{Cu-B}^{\text{III}}\text{-C}^{\text{VI}}$ compounds can accommodate large stoichiometric deviations, yielding to crystallographic structures known as ordered vacancies compounds (OVCs).

In addition, none of the investigated IPB's (consistent with the crystalline relationship experimentally deduced between both CH and CA phases) lead to the occurrence of A_4 or B_4 tetrahedral configurations. These local configurations would only occur for crystalline relationships not compatible with our experimental observations. For instance, the relative orientations $[010]_{\text{CH}}\parallel[001]_{\text{CA}}$ or $[100]_{\text{CH}}\parallel[001]_{\text{CA}}$, would lead to the formation of uncompensated IPB's between low index planes containing A_4 tetrahedra. According to the calculations of Wei *et al.*,⁷ electronic compensation between donor and acceptor clusters leads to a strong suppression of these tetrahedral configurations in disordered CH structures.

V. SUMMARY AND CONCLUSIONS

In this paper, we have analyzed the vibrational and crystallographic properties of CuInC_2 films. CA ordered domains in these films have been identified by means of electron and x-ray diffraction as well as phonon scattering. A comparison of experimental TED or HREM images and simulated images allowed identifying the orientation of an interphase

boundary between CA and CH domains. Both domains form a $(112)_{\text{CH}} \parallel (011)_{\text{CA}}$ interface. Model considerations have revealed that this interface should exhibit a compensating number of donor and acceptor type AB_3 and A_3B tetrahedra, respectively. Thus, this interface should not be charged.

In order to provide a solid basis for interpreting the Raman spectra, we have developed a VFF based model to describe the vibrational properties of the CA ordered structures of CuInS_2 and CuInSe_2 . This model predicts the position of the A_1 mode of the CA structure to be around 5% larger than the corresponding mode in the CH structure. This agrees

with the first-principles calculations performed using the frozen phonon approach. These models support the previous identification of the additional band in the Raman spectra from CA-containing films, located at 305 cm^{-1} for CuInS_2 and at 183 cm^{-1} for CuInSe_2 , with the totally symmetric mode from the CA ordered structure. Combined XRD/Raman measurements have confirmed the relationship between the intensity of these bands and the relative amount of CA phase in CuInC_2 films. The experimental results have proven the effectiveness of Raman scattering for detecting the presence of CA-ordered domains.

-
- ¹K. Siemer, J. Klaer, I. Luck, J. Bruns, R. Klenk, and D. Bräunig, *Sol. Energy Mater. Sol. Cells* **67**, 159 (2001).
- ²J. Klaer, K. Siemer, I. Luck, and D. Bräunig, *Thin Solid Films* **387**, 169 (2001).
- ³J. E. Jaffe and A. Zunger, *Phys. Rev. B* **28**, 5822 (1983).
- ⁴J. Alvarez-García, J. Marcos-Ruzafa, A. Pérez-Rodríguez, A. Romano-Rodríguez, J. R. Morante, and R. Scheer, *Thin Solid Films* **361-362**, 208 (2000).
- ⁵A. Neisser, J. Alvarez-García, L. Calvo-Barrio, R. Klenk, T. W. Matthes, I. Luck, M. Ch. Lux-Steiner, A. Pérez-Rodríguez, and J. R. Morante, in *II-IV Compound Semiconductor Photovoltaic Materials*, MRS Symposia Proceedings No. 668, edited by R. Noufi *et al.* (Materials Research Society, Warrendale, 2001), p. H1.3.1.
- ⁶J. E. Jaffe and A. Zunger, *Phys. Rev. B* **28**, 5822 (1983).
- ⁷S.-H. Wei, L. G. Ferreira, and A. Zunger, *Phys. Rev. B* **45**, 2533 (1992).
- ⁸S.-H. Wei, S. B. Zhang, and A. Zunger, *Phys. Rev. B* **59**, R2478 (1999).
- ⁹P. Fons, S. Niki, A. Yamanda, and H. Oyanagi, *J. Appl. Phys.* **84**, 6926 (1998).
- ¹⁰J. Álvarez-García, A. Pérez-Rodríguez, B. Barcones, A. Romano-Rodríguez, J. R. Morante, A. Janotti, S.-H. Wei, and R. Scheer, *Appl. Phys. Lett.* **80**, 562 (2002).
- ¹¹J. Alvarez-García, E. Rudigier, N. Rega, B. Barcones, R. Scheer, A. Pérez-Rodríguez, A. Romano-Rodríguez, and J. R. Morante, *Thin Solid Films* **431-432**, 226 (2003).
- ¹²B. J. Stanbery, S. Kincal, S. Kim, C. H. Chang, S. P. Ahrenkiel, G. Lippold, H. Neumann, T. J. Anderson, and O. D. Crisalle, *J. Appl. Phys.* **91**, 3598 (2002).
- ¹³W. H. Koschel and M. Bettini, *Phys. Status Solidi B* **72**, 729 (1975).
- ¹⁴H. Tanino, *Phys. Rev. B* **45**, 13 223 (1992).
- ¹⁵J. Lazewski, H. Neumann, K. Parlinski, G. Lippold, and B. J. Stanbery, *Phys. Rev. B* **68**, 144 108 (2003).
- ¹⁶J. Alvarez-García, A. Pérez-Rodríguez, A. Romano-Rodríguez, T. Jawhari, J. R. Morante, R. Scheer, and W. Calvet, *Thin Solid Films* **387**, 216 (2001).
- ¹⁷E. Rudigier, I. Luck, and R. Scheer, *Appl. Phys. Lett.* **82**, 4370 (2003).
- ¹⁸R. Hunger, R. Scheer, K. Diesner, D. Su, and H. J. Lewerenz, *Appl. Phys. Lett.* **69**, 3010 (1996).
- ¹⁹R. Hunger, Ch. Pettenkofer, and R. Scheer, *Surf. Sci.* **477**, 76 (2001).
- ²⁰D. S. Su, W. Neumann, R. Hunger, P. Schubert-Bischoff, M. Gier-sig, H. J. Lewerenz, R. Scheer, and E. Zeitler, *Appl. Phys. Lett.* **73**, 785 (1998).
- ²¹W. G. Fateley, F. R. Dollish, N. T. McDevitt, and F. F. Bentley, *Infrared and Raman Selection Rules for Molecular and Lattice Vibrations: The Correlation Method* (Wiley, New York, 1972).
- ²²P. N. Keating, *Phys. Rev.* **145**, 637 (1966).
- ²³R. M. Martin, *Phys. Rev. B* **1**, 4005 (1970).
- ²⁴C.-H. Chang, S.-H. Wei, S. P. Ahrenkiel, J. W. Johnson, B. J. Stanbery, T. J. Anderson, S. B. Zhang, M. M. Al-Jassim, G. Bunker, E. A. Payzant, and R. Duran (Ref. 5), p. H4.3.1.
- ²⁵J. Camassel, L. Artus, and J. Pascual, *Phys. Rev. B* **41**, 5727 (1990).
- ²⁶S. B. Zhang, S.-H. Wei, A. Zunger, and H. Katayama-Yoshida, *Phys. Rev. B* **57**, 9642 (1998).